HEFAT2012
9th International Conference on Heat Transfer, Fluid Mechanics and Thermodynamics
16 – 18 July 2012
Malta

MEASUREMENT OF PRESSURE DISTRIBUTION INSIDE A CROSS CORRUGATED HEAT EXCHANGER USING MICROCHANNEL PRESSURE TAPPINGS

Ahn C.H., Choi J., Son C., Min J.K., Park S.H., Gillespie D., Go J.S. *
*Author for correspondence
School of Mechanical Engineering,
Pusan National University,
Busan, 609-735,
Republic of Korea,
E-mail: micros@pusan.ac.kr

ABSTRACT

This paper suggests a novel method to measure pressure distribution inside a cross corrugated heat exchanger using microchannel pressure tappings. The microchannel embedded corrugated sheet is fabricated. Especially, the hydraulic diameter of the non-circular microchannel is measured. The specially designed pressure chamber is made to control the reference pressure. The pressure response is examined theoretically and experimentally in terms of delay time and peak pressure. The delay time shows linear decreases to the length of the microchannel and the peak pressure also decreases with increasing frequency of reference pressure. The microchannel pressure tapping is applicable to the steady pressure measurement but not to the transient pressure measurement. Finally, 20 corrugated sheets and one microchannel embedded corrugated sheet are stacked to form the cross corrugated heat exchanger. The static and stagnation pressures inside the heat exchanger are measured. The measured friction factor is compared with that in previous reports.

INTRODUCTION

Corrugated heat exchangers have been widely used in various engineering applications such as power stations [1,2], aero-engines [3,4] and ships [5] due to their compactness, and the high thermal efficiency that results from the increased heat transfer area and rigorous hydrodynamic mixing [6]. On the corrugated surface several patterns of embossing, ribs and herringbones have been examined for further increasing the heat transfer performance [7,8]. Specifically, the cross corrugated heat exchanger (hereafter, CCHX) has drawn attention due to requests for the development of recuperators and intercoolers for highly efficient engine systems.

Figure 1 shows a schematic of the CCHX. The corrugated sheets are stacked with an appropriate angle between adjacent sheet rows; this angle is called the chevron angle. Hot and cold sides of the heat exchanger are separated using corrugated sheets of a particular pitch to height ratio. Numerical and experimental evaluations of the thermal performance of the chevron angle and of the appropriate ratio of pitch to height of the corrugated surface have been done [9].

In most evaluations, the hydrodynamic and thermal performances of the CCHX have been examined by measuring the pressure drop and temperature difference between the inlet and outlet, as shown in Figure 2. However, in numerical design, even unit cells of the numerical domain require millions of meshes owing to their complex shape.

NOMENCLATURE

A	[m^2]	Cross sectional area of the microchannel
d	[m]	Diameter
f	[-]	Friction factor
m	[kg]	Mass
$\dot{m}$	[kg/sec]	Mass flow rate
M	[kg/mol]	Molecular mass
l	[m]	Length of microchannel and tube
L	[m]	Length of pressure tapping from CCHX inlet
R	[J/mol]	Gas constant of air
t	[sec]	Time
T	[K]	Absolute temperature
U	[m/sec^2]	Inlet velocity to CCHX
p	[Pa]	Pressure
P	[m]	Perimeter of microchannel
v	[m/sec^2]	Velocity
V	[m^3]	Volume of the microchannel

Special characters

ρ	[kg/m^3]	Density of air
μ	[kg/m·s]	Dynamic viscosity of air
τ	[sec]	Time constant

Subscripts

avg	Average
h	Hydraulic diameter
i	Inlet

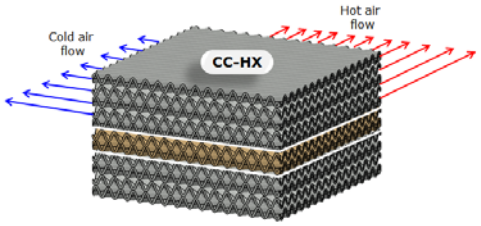

(a) The stacked cross corrugated sheets

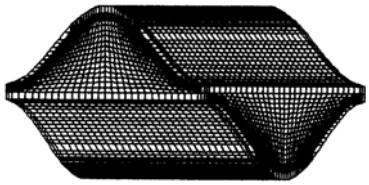

(b) Mesh generation of unit cell

Figure 1 CCHX stacked with corrugated sheets and unit cell of numerical domain.

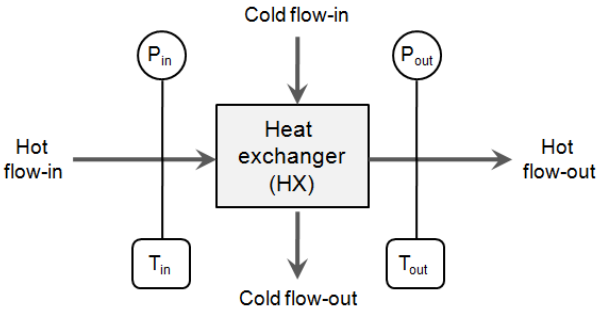

Figure 2 Diagram to characterize thermal performance of the CCHX.

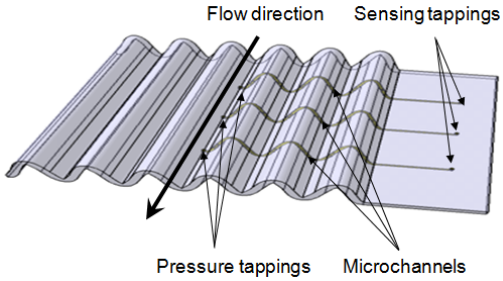

Figure 3 Schematic of a corrugated sheet embedded with microchannels to measure pressure distribution along flow direction inside the CCHX.

This means that it is not possible to extend the numerical approach to solve the full model of the CCHX. In the experimental evaluation, in order to verify the performance, the direct measurement of the pressure and the temperature can be attempted. However, the system must be manufactured in advance without knowing the field information inside the CCHX. Also, pressure and temperature can be measured only at the inlet and outlet because there is a difficulty in installing sensors inside the CCHX without disturbing the fluid flow. As a result, all the new designs must be bound with correlations of similar heat exchangers under an assumption that there is no remarkable difference in performance.

To overcome the limitations in numerical and experimental evaluation, we suggest a novel method to measure pressure distribution inside the CCHX without disturbing the flow field. Figure 3 shows a corrugated sheet that will be inserted into a stacked CCHX. Pressure tappings are integrated on the primary surface of the corrugated sheet and positioned along the flow direction. They are also interconnected to external sensing tappings by microchannels embedded in the corrugated sheet.

To test our suggestion practically, the microchannel embedded sheet is fabricated by using a diffusion bonding of two separated stainless steel sheets with chemically etched tapping holes and microchannels. The corrugation sheet is obtained by stamping the bonded plate. The pressure response of the microchannel is first investigated in terms of the delay time and peak pressure with the theoretical explanation. Then, the proposed corrugated sheet embedded with microchannels is slotted into the middle of the 20 layer stacked cross corrugated sheets and its hydrodynamic performance is characterized.

THEORETICAL PRESSURE RESPONSE OF THE EMBEDDED MICROCHANNEL

The pressure tapping to the pressure sensor is modelled as shown in Figure 4. When a pressure is applied at the pressure tapping, the pressure propagates through the microchannel and tube and reaches the pressure sensor. Then, the pressure builds up over time in the sensor volume. Because the size of the microchannel is very small, at less than 200 μm in diameter, a slow response of pressure measurement is expected, which means a long delay time.

The delay time can be driven by the mass flow rate in the Hagen-Poiseuille flow and the state equation of an ideal gas. The flow is assumed to be incompressible, 2 dimensional, steady, fully-developed and laminar. Also, the air is an ideal gas and a Newtonian fluid. As soon as the reference pressure is applied to the pressure tapping, a pressure difference is generated between the inlet of the microchannel and the pressure sensor. Thus, the air flows through the microchannel and tube until the forces are balanced.

From the Hagen-Poiseuille flow [10], the average velocity of the air flow is obtained:

$$v_{avg} = \frac{\Delta p d^2}{32 \mu l} \tag{1}$$

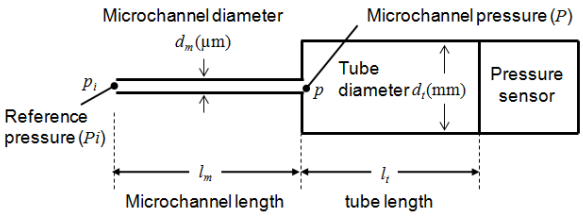

Figure 4 Modelling of the microchannel pressure measurement domain.

where d and l are the diameter and length of the microchannel and tube, respectively. Δp is the pressure difference and μ is the dynamic viscosity of air. The mass flow rate is calculated by multiplying the average velocity by the air density and cross sectional area

$$\dot{m} = \frac{dm}{dt} = \rho v_{avg} A = \rho \left(\frac{\Delta p d^2}{32 \mu l} \right) \left(\frac{\pi d^2}{4} \right) \quad (2)$$

where ρ is the air density, and A is the cross sectional area of the channel. By considering the initial air density, the mass flow rate can be modified:

$$\dot{m} = \frac{dm}{dt} = \rho v_{avg} A = \left(\frac{M p_i}{RT} \right) \left(\frac{\Delta p d^2}{32 \mu l} \right) \left(\frac{\pi d^2}{4} \right) \quad (3)$$

The mass flow rate is also obtained from the state equation of an ideal gas [11].

$$pV = \frac{m}{M} RT \quad (4)$$

$$\dot{m} = \frac{dm}{dt} = \frac{d}{dt} \left(\frac{pVM}{RT} \right) = \frac{VM}{RT} \frac{dp}{dt} \quad (5)$$

where R is the gas constant of air, T is the absolute temperature, M is the molecular mass, and V is the volume of the channel. The two mass flow rates must be equal and Δp is changed with $d(p_i\text{-}p)$.

$$-\frac{MV}{RT} \frac{d(p_i - p)}{dt} = \frac{M p_i}{RT} \frac{\pi d^4 (p_i - p)}{128 \mu l} \quad (6)$$

From the direct integration, the pressure measured at the sensor for the reference pressure can be expressed as:

$$p = p_i \left[1 - \exp\left(-\frac{t}{\tau} \right) \right] \quad (7)$$

The response time depends on the time constant, τ.

$$\tau = \frac{128 \mu l V}{\pi d^4 p_i} \quad (8)$$

The delay time depends on the time constant, so that we use the time constant as the delay time. The delay time in pressure measurement strongly depends on the diameter compared with the volume and the channel length [12]. Figure 5 shows the delay time for a 50 mm-long channel achieved by altering the diameter under the application of a reference pressure of 500 Pa. The delay time of the channel is negligible at over 0.2 mm of the channel diameter and at less than 0.2 mm it is exponentially increased. Based on a magnitude comparison, it is determined that the delay time is only considerable in the microchannel, while the delay time in the millimetre scale tube is negligible.

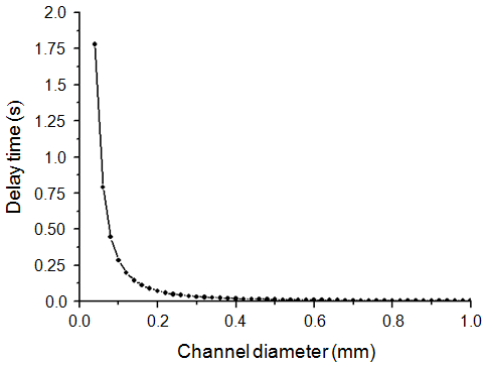

Figure 5 Time delay with varying diameter of channel.

FABRICATION OF THE MICROCHANNEL-EMBEDDED CORRUGATED SHEET

The microchannel embedded corrugated sheet was fabricated by three main steps of metal etching, diffusion bonding and mechanical stamping. The typical thickness commercially available for these plates is on the order of 100 μm. This compares well with the desired value used in a real scale heat exchanger of approximately 100 μm. Two separated stainless steel plates (SUS-304) each with thickness of 100 μm were prepared. One plate was etched through to make holes to form the pressure tappings and the sensing tappings. Another plate was partly etched to form the microchannels. Ferric chloride solution, $FeCl_3$ was used to etch the SUS-304 plates [13]. The diameter of the through-etched hole was set at 400 μm by considering the isotropic etching profile of metal etching. The width and depth of the partly etched microchannel were 300 μm and 50 μm, respectively. Microchannels with six different lengths of 43 mm, 49 mm, 55 mm, 61 mm, 68 mm, and 74 mm were designed in order to measure the pressure distribution along the flow direction. Figure 6 provides a cross sectional view and the sizes of the two etched plates.

In the next process, after the pressure tapping holes were aligned above the microchannels to allow for fluidic connections, the two etched plates were placed in a vacuum furnace and were bonded using diffusion bonding to form the microchannels and tappings [14]. The bonding was carried out at the high temperature of 1000 ^{o}C and with a load of 10 MPa. To investigate the bonding quality, water leakage was tested. Deionized water was infused into one microchannel by using a syringe and the water was observed only at the outlet connected with that microchannel (Fig. 7). After that, the outlet was closed and the water was infused again into that microchannel. The water was not observed in neighboring microchannels. This means that hermetic and reliable bonding of the two plates was obtained.

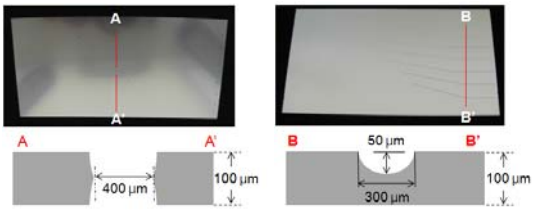

(a) Hole plate (b) Microchannel plate

Figure 6 Two etched plates and their cross sectional views.

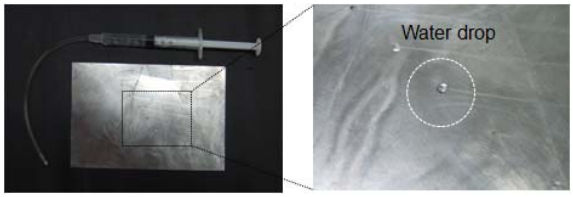

Figure 7 Hermetic bonding of two etched plates and water leak test

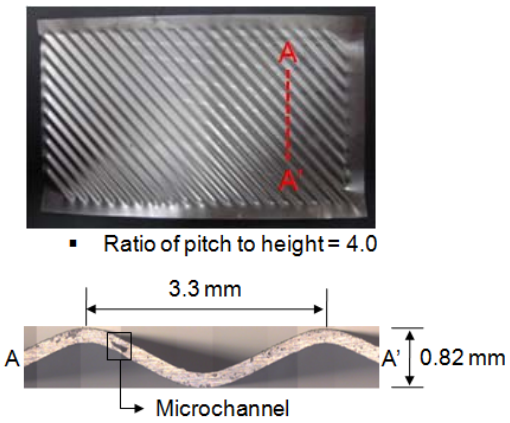

Figure 8 The microchannel-embedded corrugated sheet with a ratio of 4.0

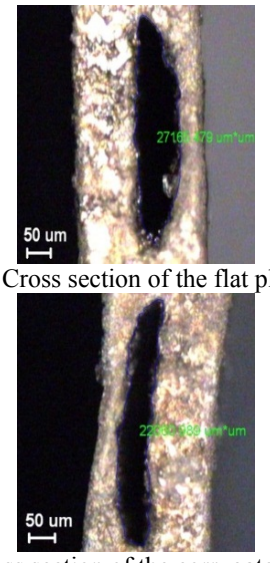

(a) Cross section of the flat plate

(b) Cross section of the corrugated plate

Figure 9 Measurement of perimeter and area of the microchannel

In the final process, the bonded flat plate was corrugated by mechanical stamping. In order to obtain a ratio of pitch to height of 4.0 without breaking the microchannels, the holding force and stamping force were set at 4 MPa and 6 MPa, respectively. A corrugated plate, with the pitch of 3.3 mm and a height of 0.82 mm, was formed, resulting in a ratio of 4.0. Figure 8 shows the corrugated sheet and the embedded microchannel clearly in the cross sectional view.

The precise measurement of the diameter is required because the delay time depends on the fourth power of the diameter of the microchannel. However, the cross section of the microchannel is not like a circle or a rectangle, as shown in Figure 9. In general, the diameter of a non-circular channel can be defined as a hydraulic diameter,

$$d_h = \frac{4A}{P} \tag{9}$$

where A is the cross sectional area of the microchannel and P is the length of its perimeter.

To measure the hydraulic diameter, we used a commercial program (iSolution Lite). First, the microchannel was cut into 10 pieces along the distance. The cross section of these pieces was photographed with a high resolution CCD camera (VCC-6574A, Sanyo) installed in a microscope (MX51, Olympus). A CCD image generally contains 2-dimensional digital pixels. By counting the pixels accommodating the area and the perimeter and converting them into scale by using a reference scale bar, the hydraulic diameter can be calculated.

Figure 10 shows the quantitative measurement of the average hydraulic diameter and the standard deviation of the six different microchannels. The hydraulic diameter decreased about 10.5 % after the stamping process. The overall average hydraulic diameter of the flat plate was 119 μm, with a standard deviation of 8.1 μm. The overall average hydraulic diameter of the corrugated microchannel was decreased to 106 μm and the standard deviation was increased to 14.3 μm. The large standard deviation was a result of the valley or floor positions of the cross sections of the microchannel.

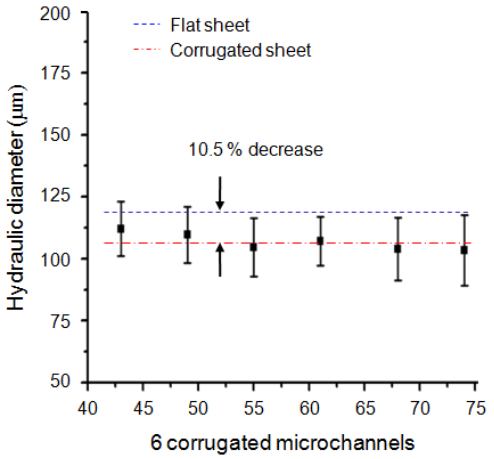

Figure 10 Quantitative measurement of the hydraulic diameters and their size distribution.

EXPERIMENTAL EVALUATION OF PRESSURE RESPONSE OF MICROCHANNELS

To determine the efficiency of nanocapsule and acetone PLGA fractionation we analyzed samples from the three outlet channels using optical transmittance and mass measurements. Samples fractionated into the center and two side outlets were collected, and their mass was measured using a high-precision mass-scale instrument (HR-200, A&D). The ratios of the volume collected from each side outlet to that collected from the center outlet were 1.285 and 1.290 *ml*, respectively. This shows good agreement with the numerical flow rates ratio of 1.25 and suggests that only a small portion of the polymerized nanocapsules were collected through the two side-outlet channels.

For the experimental characterization of the pressure response of the microchannel, the pressure chamber was specially designed to control the reference pressure. Figure 11 shows the pressure control chamber, which consisted of a chamber with an initial volume of 80 *ml*, a PZT disk (T216-A4NO-573X, Piezo Systems) with a diameter of 100 mm, a tube with a diameter of 5 mm connected to a reference pressure sensor, and the microchannel-embedded plate connected to the pressure sensors.

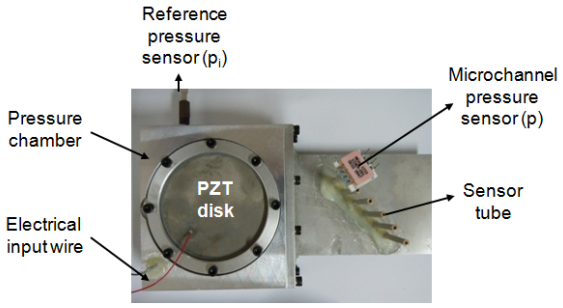

(a) Pressure control chamber

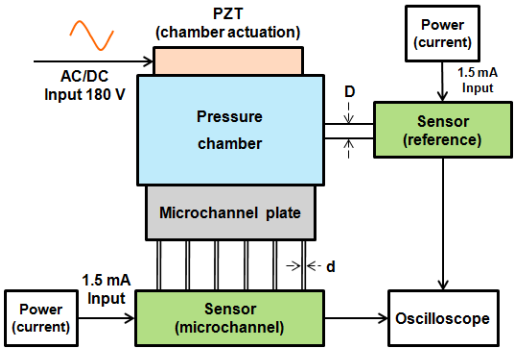

(b) Operation diagram

Figure 11 Picture of the pressure chamber and its operation diagram

The operation diagram showing how the pressure response was measured is also given. The maximum applicable voltage was found through experiment to be 180 V, which value was limited by the breakdown voltage of the PZT disk. When an electrical input of 180 V is applied to a PZT disk, the disk deforms statically or dynamically according to the DC or AC input. Then, the volume of the pressure control chamber changes with the displacement of the PZT disk. As a result, the reference pressure in the pressure chamber can be altered and measured in the reference pressure sensor (1210_1 psi, Measurement Specialties). The delay time in the tube is negligible because of the large diameter. By synchronizing the reference pressure sensor and the microchannel pressure sensor in time, an oscilloscope reads both pressures simultaneously.

First, for the step-wise input of the reference pressure, the pressure response was characterized. The input voltage of DC 180 V was applied to the PZT disk. Then, it deformed statically downward to 476 μm. The chamber pressure was measured at 430 Pa, as determined by the reference pressure sensor (Fig. 12). The pressure propagated through the microchannel and the pressure started to build up slowly in the pressure sensor due to the strong viscous friction in the microchannel and the large volume in the tube. As a result, the expected delay time occurred between the reference pressure and the microchannel pressure. We measured the delay time when the pressure reached 63.2 % of its final value.

Figure 13 shows the average delay time with an error bar obtained from the five repeated experiments. Also, this figure compares the measured delay time to the value that was calculated theoretically. Specifically, the theoretical delay time was calculated using Eq. (8) by inserting the measured average hydraulic diameter. The results show good agreement with the theoretical behavior in that the delay time increases proportionally to the increasing length of the microchannel. However, there is still a discrepancy between the two values, which is thought to result from the large distribution of the hydraulic diameter and the corrugation of the microchannel.

Second, the dynamic pressure response was measured in order to evaluate the possibility of transient pressure measurement using microchannel pressure tapping. To situate the periodic change of the pressure in the pressure chamber, the AC input of 180 V was applied to the PZT disk by altering the frequency. The vibrating displacement resulted in a harmonic change of the reference pressure. Figure 14 compares the dynamic pressure response of the microchannel for the harmonic pressure input. Not only the delay time but also the magnitude of the peak pressure was reduced. The peak pressure is the peak-to-peak value of the pressure measured in the microchannel sensor. The delay time measures the lag for the input pressure.

Figure 15 shows the dynamic pressure response achieved by increasing the frequency of the reference pressure. The frequency was increased from 1 Hz to 5 Hz. The magnitude of the peak pressure and the delay time in the microchannel were measured. Both of these values decreased with the increasing frequency. The reason why the peak pressure decreased for increasing frequency can be explained. For example, for the reference pressure of 1 Hz, it takes 0.25 seconds to reach the

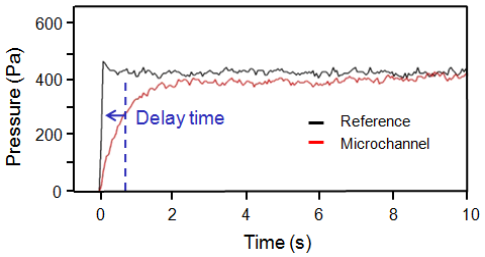

Figure 12 Pressure response of the microchannel of 43 mm for step change of the chamber pressure

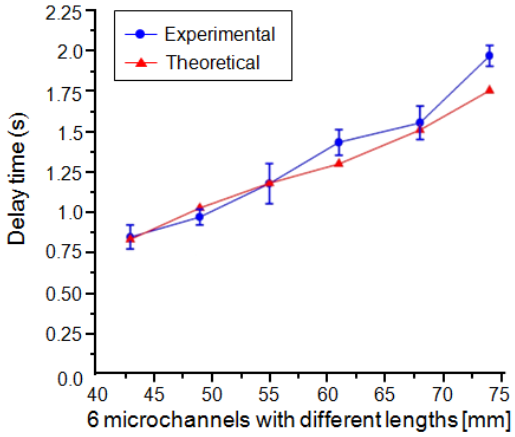

Figure 13 Delay times of six different microchannels in flat and corrugated sheets

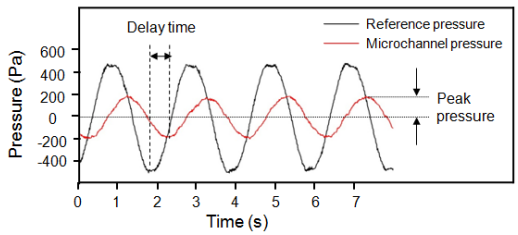

Figure 14 Dynamic pressure response for periodic change of the chamber pressure

maximum pressure of 430 Pa. There must be a delay time in the pressure response. We can read the pressure corresponding to the time of 0.25 seconds from the measured pressure response in the corrugated microchannel for the step pressure change. For the corrugated microchannel of 43 mm, a peak pressure of about 150 Pa was read, while a peak pressure of 187 Pa was measured in the experiment.

The delay time is also reduced rapidly for increasing frequency because the time period becomes shorter. We examined the rate percentage of the delay time. This percentage was defined as the ratio of the delay time to the time period of the input frequency. It is interesting that a fairly constant rate percentage of 24 % was measured for all lengths and input frequencies, as shown in Figure 15(b).

The measurement of the dynamic pressure response of the corrugated microchannel indicates that it is difficult to apply microchannel pressure tappings to measure the transient pressure, which pressure changes quickly with time.

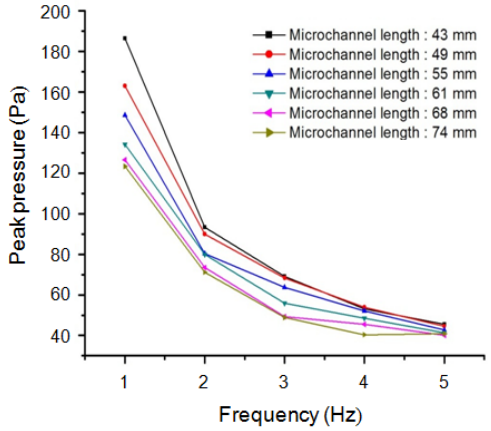

(a) Peak pressure

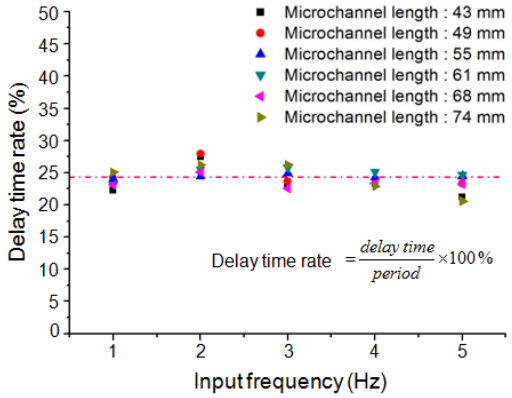

(b) Delay time rate

Figure 15 Dynamic pressure response of the microchannels in the corrugated sheet for varying frequency

APPLICATION TO THE MEASUREMENT OF PRESSURE DISTRIBUTION IN THE CCHX

Microchannel pressure tappings were applied to measure the static pressure distribution inside CCHX. The 21 corrugated sheets, comprised of the 20 dummy corrugated sheets and the one microchannel embedded sheet were stacked with a chevron angle of 90°. The microchannel corrugated sheet was slotted into the middle of the CCHX. The integrated pressure tappings on the corrugated surface allowed us to measure the pressure distribution inside the CCHX.

A single blow wind tunnel was prepared. Every effort was made to ensure that the flow field was as uniform as possible; this was done by inserting honey combs and meshes in a wind tunnel. Also, mal-distribution in the test section was minimized. A Pitot tube was equipped with instrumentation to measure the inlet and outlet velocities; this tube was positioned 30 cm away from the test section of the CCHX.

In this experiment, owing to the limitations of the blower, reliable velocities in the wind tunnel were obtained at 6.86 and 7.76 m/s, respectively. By using the hydraulic diameter obtained from the pitch and height formed by stacking the corrugated sheets, the Reynolds number values of the air flow were calculated at 698 and 790 respectively.

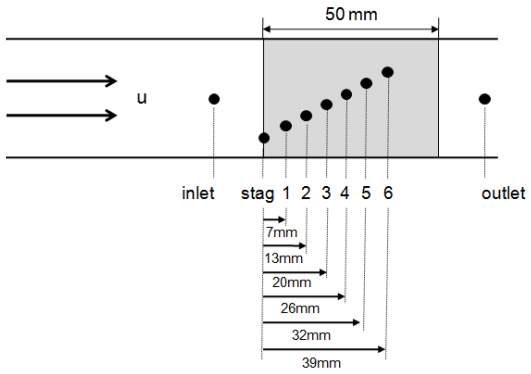

Figure 16 Experimental setup for pressure distribution measurement of the 21 layer stacked CCHX

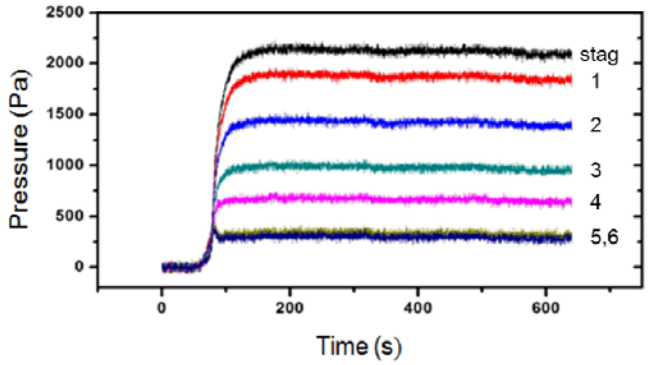

(a) Reynolds number of 698

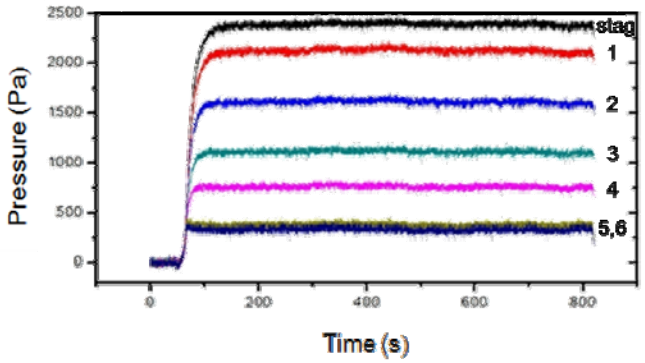

(b) Reynolds number of 790

Figure 17 Average pressure measurement inside CCHX at nine different positions

The pressure was measured at nine positions. The static pressures were measured at the inlet and outlet of the test section and at the six pressure tappings inside the CCHX along the flow direction. Also, the pressure tapping at the leading edge of the plate was used to measure the stagnation pressure. The pressure measurement positions are indicated in Figure 16.

Figure 17 shows the measured pressures in the time domain at Reynolds numbers of 698 and 790. The figure also shows that the pressure does not change over at a time. The pressure was larger at the high Reynolds number flow than at the small Reynolds number flow.

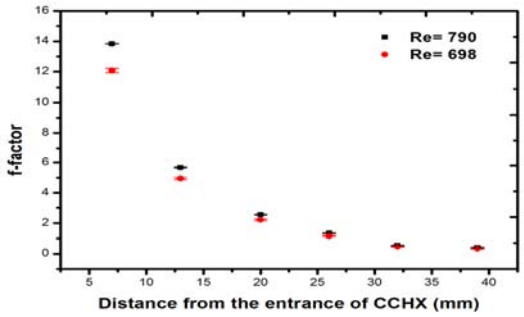

Figure 18 Calculation of f factor along the flow passage

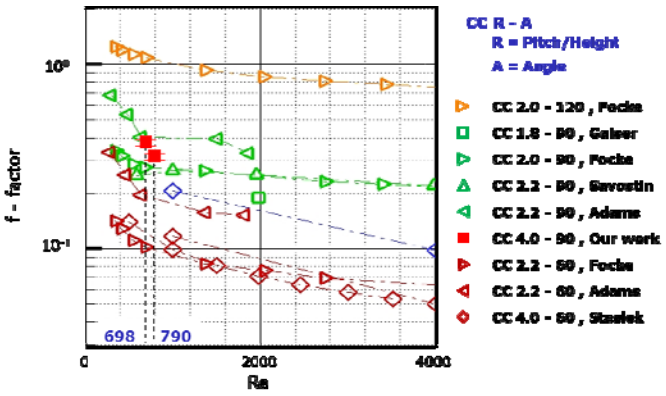

Figure 19 Comparison of the measured friction factors with those of previous works

The pressure was read when the pressure showed the saturation for 5 minutes. Measurement has been done 3 times. The maximum pressure is obtained at the stagnation pressure tapping and the static pressure is decreased approximately in proportion along the flow direction.

To examine the characteristics of pressure drop, the friction factor was calculated to distance. As shown in Fig. 18, the friction factor is saturated as being away from the entrance. This indicates an entrance effect [15]. If the flow is laminar, the entrance length is calculated to be 41.8 and 47.4 mm for the Reynolds number of 698 and 790. If the flow is turbulent, the entrance length is calculated to be 13.3 and 13.4 mm for the Reynolds number of 698 and 790 respectively. A previous work reported that the flow is turbulent even at the Reynolds number of 200 in the cross corrugated flow passage [16]. However, since the microchannel pressure tapping cannot sense the transient change of pressure, no fluctuation of the pressure was found. This also implies that whether the flow is laminar or not turbulent, there must be an entrance effect.

$$f = \Delta p\left(\frac{d_h}{L}\right)\left(\frac{2}{\rho U^2}\right) \tag{10}$$

When the friction factor was saturated to a constant, as shown in Figure 19, the friction factor was obtained and compared with those obtained from previous works [17~20]. The ratio of pitch to height can be considered, as can the chevron angle. It is shown that the friction factor is more

strongly dependent on the chevron angle than it is on this ratio. Our measurement of the friction factor is also well positioned in the range of the same angle of 90°. This implies that the microchannel pressure tapping enables us to measure the static pressure distribution inside the CCHX without any flow disturbance.

CONCLUSIONS

The pressure distribution inside a cross corrugated heat exchanger has been successfully measured by using microchannel pressure tappings. A fabrication method for the microchannel embedded sheet is also introduced: the method uses metal etching, diffusion bonding and stamping. The hermetic bonding of the microchannel embedded plates is guaranteed by a water leak test. The overall hydraulic diameter of the corrugated microchannel was 106 μm, with a standard deviation of 14.3 μm. In order to characterize the pressure response of the microchannel, a pressure chamber that can enable the control of the reference pressure is specially designed and made.

From the theoretical and experimental evaluation of the pressure response of the microchannel, the delay time and the reduction of the peak pressure were measured for the static and dynamic change of the reference pressure. The microchannel pressure tapping method is more appropriate for the measurement of the static pressure than for the measurement of the transient pressure because the pressure is hardly measurable at a frequency of 5 Hz. In addition, the application of the microchannel pressure tapping to the CCHX and the success of this process imply that a practical design of the CCHX is possible with a numerical analysis of the unit cells, performed by providing the experimental static and stagnation pressures.

For further work, more experiments must be done on pressure distribution along and transverse to the flow direction. Also, in order to allow an anticipation of the delay time for an increasing frequency, a dynamic model of the vibration of air in the microchannel due to the periodic change of pressure difference will be determined.

ACKNOWLEDGEMENT

This research was supported by Leading Foreign Research Institute Recruitment Program through the National Research Foundation of Korea (NRF), funded by the Ministry of Education, Science and Technology (MEST) (No.K20703001798-11E0100-00310), this work was supported by the National Research Foundation of Korea (NRF) grant funded by the Korea government (MEST) (No. NRF-2011-0017011)

REFERENCES

[1] Stasiek J., Collins M.W., Ciofalo M., Chew P.E., Investigation of flow and heat transfer in corrugated passages – I. Experimental results, *Int. J. Heat Transfer*, Vol. 39, No.1, 1996, pp.149-164

[2] Aquaro D., and Peive M., High Temperature heat exchangers for power plant: Performance of advanced metallic recuperators, *Applied Thermal Engineering*, Vol. 27, 2007, pp.389-400

[3] Min J. K., Jeong J. H., Ha M. Y., Kim K. S., High temperature heat exchanger studies for applications to gas turbines, *Heat and Mass Transfer*, Vol. 46, No.2, 2007, pp.175-186

[4] Reay D.A., Compact heat exchangers: A review of current equipment and R&D in the field, *Heat Recovery Systems and CHIP*, Vol. 14, No.5, 1994, pp.459-474

[5] Cicek K., and Celik M., Selection of porous materials in marine system design: The case of heat exchanger aboard ships, *Materials & Design*, Vol. 30, No.10, 2009, pp.4260-4266

[6] Dubrovsky E.V., Experimental investigation of highly effective plate-fin heat exchanger surfaces, *Experimental Thermal and Fluid Science*, Vol. 10, No.2, 1995, pp.200-220

[7] Rafferty K.D., and Culver G., Heat Exchanger, *Geo-Heat Center Klamath Falls*, Oregon 97601

[8] Kondepudi S.N., O'Neal D.L., Frosting performance of tube fin heat exchangers with wavy and corrugated fins, *Experimental Thermal and Fluid Science*, Vol. 4, No.5, 1991, pp.613-618

[9] Park J.H., Characteristics and Applications of Plate Type Heat Exchanger, *The Korean Society of Marine Engineering*, Vol. 33, No.6, 2009, pp. 801-811

[10] Islamoglu Y., Parmaksizoglu C., The effect of channel height on the enhanced heat transfer characteristics in a corrugated heat exchanger channel, *Applied Thermal Engineering*, Vol. 23, No.8, 2003, pp.979-987

[11] Schmid P.J. and Henningson D.S., Optical energy density growth in Hagen-Poiseuille flow, *Journal of Fluid Mechanics*, Vol. 277, 1994, pp.197-225

[12] Wark K., Adanced thermodynamics for engineers international editions, *McGraw-Hill*, New York, 1995

[13] Xie H.Y., Geldart D., The response time of pressure probe, *Powder Technology*, Vol. 90, 1997, pp149-151

[14] Cho M.S., Lim H.W., Lee C.S., Cho B.K., Cho Y., Park J.G., Fabrication of Stainless Steel Mold using Electro Chemical Fabrication (ECF) method for Microfluidic Biochip, *Microprocesses and Nanotechnology*. 2007, pp.334-335

[15] Ghosh M., Bhanumurthy K., Kale G. B., Krishnan J., Chatterjee S., Diffusion bonding of titanium to 304 stainless steel, *Journal of Nuclear Materials*, Vol. 322, 2003, pp.235-241

[16] Munson B.R., Young D.F., Okiishi T.H., Fundamental of Fluid Mechanics, *John Wiley & Sons, New York*, 2006

[17] Focke W.W., Zachariades J., Olivier I., The effect of the corrugation inclination angle on the thermohydraulic performance of plate heat exchangers, *Int. J. Heat Mass Transfer*, Vol. 28, No.8, 1985, pp.1469-1479

[18] Gaiser G. and Kottke V., Flow phenomena and local heat and mass transfer in corrugated passages, *ChemEng Technol*, Vol.12, No.1, 1989, pp.400-405

[19] Adams j., Advanced Heat Transfer Surfaces for Gas Turbine Heat Exchangers, *Ph. D Thesis*, University of Oxford, 2004

[20] Stasiek J. A., Experimental studies of heat transfer and fluid flow across corrugated-undulated heat exchanger surfaces, *Int. J. Heat Mass Transfer*, Vol. 41, Issues.6-7, 1998, pp.899-914